JOURNAL OF GUIDANCE, CONTROL, AND DYNAMICS
Vol. 24, No. 4, July–August 2001

Tuning of Coning Algorithms to Gyro Data Frequency Response Characteristics

J. G. Mark* and D. A. Tazartes†
Litton Guidance and Control Systems, Woodland Hills, California 91367

Substantial efforts have gone into the development of sophisticated algorithms that reduce system drift errors in the presence of coning motion. Present-day algorithms form high-order coning correction terms using multiple incremental angle outputs from the gyros. These algorithms assume a flat transfer function for the processing of the incremental angle outputs and are structured to yield very high-order responses. However, these algorithms do not address the issue of nonideal gyro frequency response or of filtered gyro data. Many gyros exhibit complex frequency responses and violate the assumptions used in deriving the previously developed coning algorithms. The mismatch between the assumed and actual frequency response of the gyro data leads to degradation of performance in a coning environment as well as amplification of pseudoconing errors. A method of deriving algorithms that are tailored to the frequency response of the particular type of gyros used is presented. These algorithms can be designed to arbitrarily high order and can also supply an extremely sharp high-frequency cutoff to minimize pseudo-coning errors. Additionally, this method can be used to design coning algorithms that are tuned to deliberately filtered gyro data. The technique developed equally applies to mechanical, fiber-optic, and other types of gyros.

Introduction

In a strapdown inertial navigation system, angular rotation measurements are processed and integrated to form an attitude quaternion or matrix that describes the attitude of the system with respect to a stabilized reference coordinate system. Attitude integration is complicated by the noncommutativity of rotations and by finite instrument sampling rates. This becomes a problem if the axis of rotation changes directions dynamically. In this case, it can be easily shown that the attitude of a body depends not only on the magnitude but also on the order of the rotations performed. If the order is not properly tracked, then attitude errors will result, and navigation performance will be seriously degraded. Coning motion is one particular input used to evaluate strapdown inertial navigation systems and attitude integration algorithms. Coning is a demanding type of motion, and algorithms that operate satisfactorily in this environment will satisfy most other requirements. In coning motion, one (or more) axes of the system sweeps out a cone in space. The Goodman–Robinson theorem[1] states that the output of a gyro whose sensitive axis is along a coning axis will be equal to the solid angle swept by this axis, even though there is no net rotation produced. An appropriate attitude integration algorithm can process three axes of information from orthogonal gyros and reconstitute the actual motion. However, an additional complication lies in that, in practice, instrument (gyro) outputs are only sampled at finite rates. The sampling bandwidth limitation must, therefore, be taken into account. In the past, coning algorithms have been used to improve attitude integration algorithms using sampled gyro data. These algorithms are discussed in several references, such as Refs. 2–7. However, these publications deal with ideal gyroscopes. In many instances, gyro outputs have a shaped frequency response or are filtered to reduce other errors such as quantization[8] or vibration-induced errors. In these cases, the traditional coning algorithms do not work to high-order accuracy. Pseudoconing is an additional concern. For example, some types of gyroscopes respond to high-frequency vibration and generate erroneous high-frequency outputs. These erroneous outputs, combined with true angular motion at the same frequency, will cause an erroneous coning correction and will actually amplify this pseudoconing error. Paradoxically, the more effective and wideband the coning algorithm, the more pseudoconing error will be generated. The use of appropriately filtered data and properly tuned coning algorithms provides the added benefit of reduced pseudoconing error by permitting a sharp cutoff in the coning algorithm response. This paper discloses a method of tuning high-order coning algorithms to match the frequency response characteristics of the gyroscopes or of the filters used to preprocess the gyroscope data. These algorithms achieve high-order corrections despite nonideal gyro frequency response while also exhibiting sharp cutoffs.

Coning Algorithms

The usual method of generating high-order coning algorithms, that is, algorithms that approach ideal coning response, begins with a postulated coning motion about the z axis as described in the first part of the Appendix. Each attitude update requires a vector angle $\Delta \boldsymbol{\phi}$, which is a single-axis rotation describing the net attitude change from the beginning to the end of the interval in question. The problem is in that the gyro incremental angle outputs $\Delta\theta$ are only an approximation to the components of the required vector angle. To improve the approximation, each attitude integration interval is divided into m subintervals of equal duration. Gyro data samples from the subintervals are processed to yield a high-order approximation of the vector angle. The correction $\Delta \boldsymbol{\phi} - \Delta \boldsymbol{\theta}$ is formed by combining cross products of the $\Delta \boldsymbol{\theta}_i$ of the m subintervals. Figure 1 shows an example for the case $m = 4$.

In this case, there are six possible vector cross products that can be formed, and these are grouped in three different categories depending on the spacing between the data samples: spacing 1, $\Delta \boldsymbol{\theta}_1 \times \Delta \boldsymbol{\theta}_2$, $\Delta \boldsymbol{\theta}_2 \times \Delta \boldsymbol{\theta}_3$, and $\Delta \boldsymbol{\theta}_3 \times \Delta \boldsymbol{\theta}_4$; spacing 2, $\Delta \boldsymbol{\theta}_1 \times \Delta \boldsymbol{\theta}_3$, and $\Delta \boldsymbol{\theta}_2 \times \Delta \boldsymbol{\theta}_4$; and spacing 3, $\Delta \boldsymbol{\theta}_1 \times \Delta \boldsymbol{\theta}_4$.

In general, there are $m - 1$ possible spacings and C_m^2 possible vector cross products (VCP). Each category of cross products is described by the quantity $C_p(n)$, where

$$C_p(n) = (\Delta \boldsymbol{\theta}_{nm} \times \Delta \boldsymbol{\theta}_{nm+p})_{\boldsymbol{k}\text{th component}} \tag{1}$$

It can be shown that all cross products with the same spacing have the same $\boldsymbol{k}$ component and that the result for $C_P(n)$ is independent of n. The time-varying (ac) components, that is, $\boldsymbol{i}$ and $\boldsymbol{j}$, have only higher-order terms and can be ignored. The coning correction is formed by taking a linear combination of C_P that approximates the difference between $\Delta \boldsymbol{\phi}$ and $\Delta \boldsymbol{\theta}$. Compensation can be achieved to an order commensurate with m. That is, the relative residual error behavior is up to the $(2m)$th power of frequency. Methods of solving for the coefficients of the C_P are given in several references, including Refs. 4 and 5. These methods expand the coning error

Received 3 June 1999; revision received 18 October 2000; accepted for publication 1 November 2000.

*Technical Advisor.
†Chief Technology Officer.

Table 1 Standard coning algorithm coefficients

Number of subintervals M	Order	Cross-product distance	Cross-product coefficient	Residual error coefficient
1	2	N/A	N/A	$-1/3!$
2	4	1	2/3	$-4/5!$
3	6	1	27/20	$-36/7!$
		2	9/20	
		1	214/105	
4	8	2	92 / 105	$-576/9!$
		3	54/105	
		1	1375/504	
5	10	2	650 /504	$-14{,}400/11!$
		3	525/504	
		4	250/504	

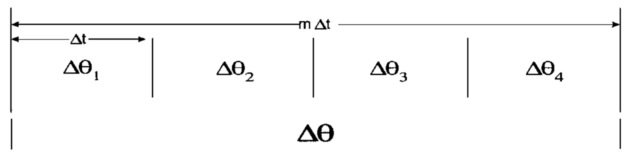

Fig. 1 Gyro data intervals.

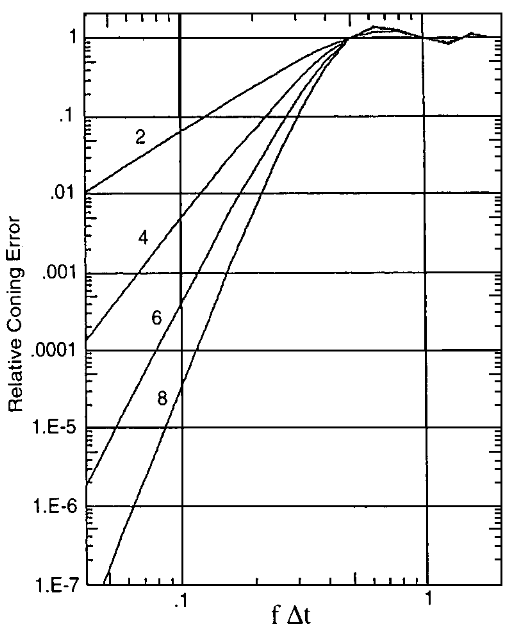

Fig. 2 Standard coning algorithm error response.

$(\Delta\,\phi - \Delta\,\theta)_{k\text{th component}}$ and cross-product families C_P into Taylor series expressed in terms of powers of frequency. The first m terms of the coning error series are equated to the corresponding terms of a linear combination of cross products, and the coefficients applying to those cross products are solved for. Thus, the error corresponding to the first m terms in the coning error expansion are completely compensated. For example, for a four-sample algorithm, that is, $m = 4$, the ideal coning correction is given by

$$\Delta\,\phi \approx \Delta\,\theta + (1/105)(214\mathbf{VCP}_1 + 92\mathbf{VCP}_2 + 54\mathbf{VCP}_3)$$

where

$$\mathbf{VCP}_1 = a\Delta\,\theta_1 x\Delta\,\theta_2 + b\Delta\,\theta_2 x\Delta\,\theta_3 + c\Delta\,\theta_3 x\Delta\,\theta_4 \quad a+b+c=1$$

$$\mathbf{VCP}_2 = d\Delta\,\theta_1 x\Delta\,\theta_3 + e\Delta\,\theta_2 x\Delta\,\theta_4 \quad d+e=1$$

$$\mathbf{VCP}_3 = f\Delta\,\theta_1 x\Delta\,\theta_4 \quad f=1$$

Table 1 summarizes the VCP coefficients for the first five algorithms.The corresponding coning error relative residual plots are given in Fig. 2 where f is the coning frequency and Δt is the sample interval for the angle increments.

Note that the algorithm frequency response follows the $(2m)$ order discussed earlier. Furthermore, the algorithms essentially cut off at the Nyquist frequency ($f\,\Delta t = \frac{1}{2}$) and some overshoot (error amplification) occurs between the Nyquist frequency and the sampling frequency. This results from the usual aliasing problems occurring with sampled data. In general, we would like as sharp a cutoff as possible to maintain coning rejection at lower frequencies along with the minimum amplification of errors above the Nyquist frequency. Some instruments also exhibit pseudoconing, that is, an erroneous high-frequency output, which does not reflect true physical motion. It is, therefore, desirable to cut off sharply the frequency response of the coning algorithm to avoid compensation of an apparent (not real) coning motion.

Coning Algorithm for Frequency-Shaped Gyro Data: Example

An excellent example of frequency-shaped gyro data is that discussed in Ref. 8, where a resolution-enhancement technique that can be applied to laser gyroscopes is discussed. What is described is a method of reducing quantization noise by using a digital antialiasing filter. This filter, which operates with high-speed sampling, greatly improves the resolution but also shapes the frequency response of the data. This example is chosen because of the simplicity of the filter's transfer function. It is also a real application of the technique described in this paper. A completely general treatment is also pursued in the Appendix. The transfer function of the resolution-enhancement frequency shaping[8] is given by

$$F(\omega) = \frac{\sin\left(\frac{1}{2}\omega\Delta t\right)}{\frac{1}{2}\omega\Delta t} \tag{2}$$

where ω is the coning (angular) frequency and Δt the sampling interval for the angle increments.

If the resolution-enhanced data are used, each incremental angle will be shaped by the preceding response function as a function of frequency. This, in turn, affects the series expansion of the VCPs that are created from the incremental angles. That is, each of the VCPs described earlier will have a different series expansion in terms of frequency.

The VCP coefficients shown in Table 1 were derived in the case of an ideal incremental angle frequency response. These will no longer be applicable in the case of the frequency-shaped data. If used in a coning algorithm with resolution-enhanced data, these coefficients

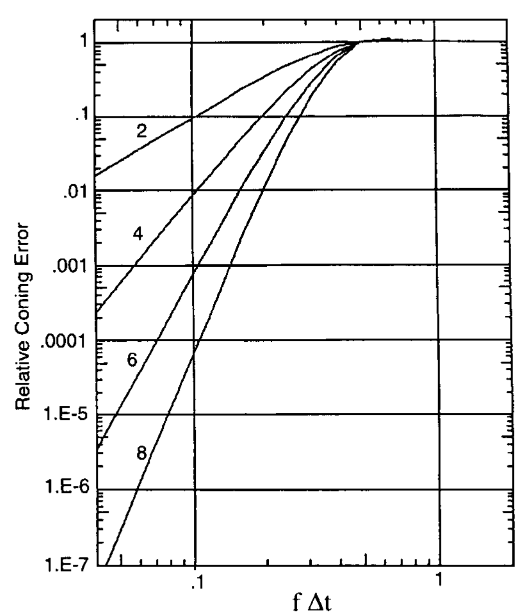

Fig. 3 Coning error response for algorithms tuned for resolution-enhanced data.

will result in significantly degraded coning performance. Nonetheless, using the technique derived in the Appendix, it is possible to derive modified coefficients that are specifically tuned to the filter transfer function of Eq. (2). These coefficients are given in Table 2 for two, three, four, and five sample algorithms. These could of course be computed for any number of samples.

Figure 3 shows the relative coning error response for these algorithms (tuned for resolution-enhanced data) as a function of frequency. Note that the residual error coefficients are slightly larger than in the case of unfiltered data but only marginally so. The coning response is again seen to cut off at the Nyquist frequency. However, the cutoff is much sharper with much less overshoot, that is overcompensation, beyond the Nyquist frequency. These algorithms, therefore, take advantage of the band limiting provided by the data prefiltering thereby avoiding aliasing as well as pseudoconing errors.

Figures 4 and 5 were additionally generated to compare the coning algorithm frequency response (as opposed to relative error response). Figure 4 shows the coning algorithm response for the four-sample eighth-order algorithm operating on unfiltered data. Figure 5 shows the four-sample, eighth-order algorithm response using resolution-enhanced data with appropriate tuning. Comparison of Figs. 4 and 5 clearly illustrates how the filtered data algorithm provides a much sharper cutoff.

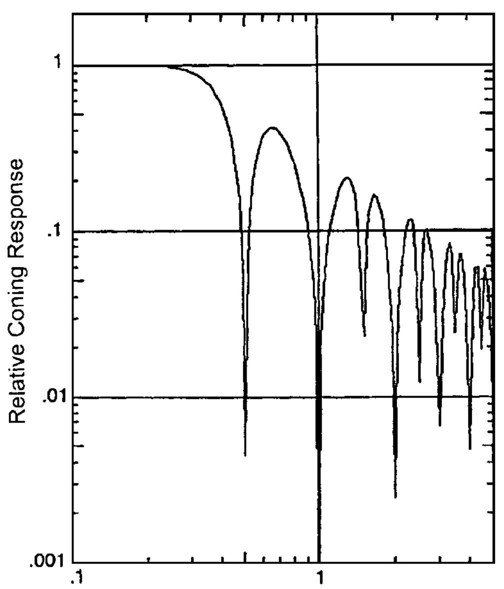

Fig. 4 Standard coning algorithm response.

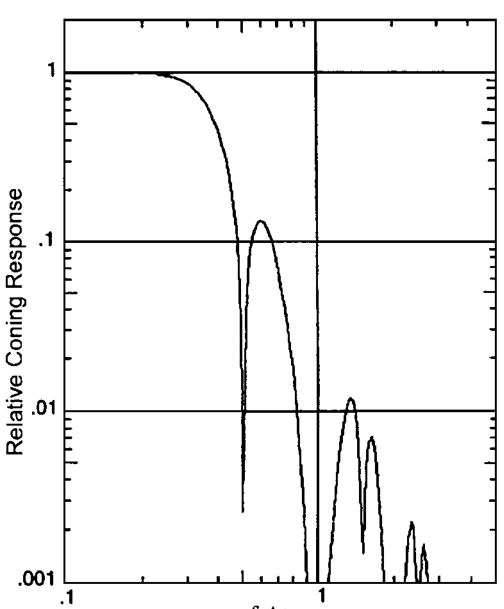

Fig. 5 Resolution-enhanced coning algorithm response.

Table 2 Coning algorithm for resolution-enhanced data

Number of subintervals M	Order	Cross-product distance	Cross-product coefficient	Residual error coefficient
1	2	N/A	N/A	−30/5!
2	4	1	3/4	−294/7!
3	6	1	124/80	−4,920/9!
		2	33/80	
		1	17,909/7,560	
4	8	2	5,858/7,560	−124,456/11!
		3	3,985/7,560	
		1	193,356/60,480	
5	10	2	66,994/60,480	−4,638,816/13!
		3	65,404/60,480	
		4	29,762/60,480	

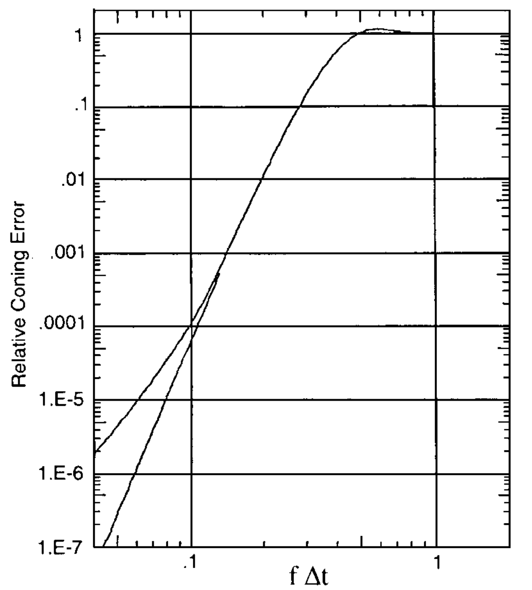

Fig. 6 Resolution-enhanced coning error response for large motions.

Simulation

To verify the proper operation of the coning algorithms, a simulation was constructed and a coning motion was applied to the algorithms. The results agree with the predictions. In fact, Figs. 1 and 2 are the result of simulation, and the slopes agree with the theoretical predictions given in the last column of Tables 1 and 2, respectively. In addition, an eighth-order algorithm ($m = 4$) simulation with very high coning rates was also attempted. This case is shown in Fig. 6 for the resolution-enhanced data condition. Figure 6 shows excellent agreement with the lower coning rate case with deviations only occurring at low frequency, where the angle excursions of the cone are extremely large. Even so, the algorithm does not break down but smoothly transitions to a lower order.

General Case

The example presented in the preceding section applies to the frequency response of the resolution enhancement filter described in Ref. 8. However, the technique can be applied in general to any frequency-response function that approaches unity at zero frequency and that remains bounded for all frequencies. The Appendix provides a generalized set of equations, which can be used to determine the properly tuned coning algorithm coefficients for any frequency-response function meeting these criteria. The method simply involves equating term-by-term the coefficients of the series expansion of the coning compensation obtained using the filtered gyro data on one hand and those of the desired coning compensation on the other. The prescribed method results in a system of linear equations, which can be solved for the appropriate set of coning algorithm coefficients. The solution to the system of Eqs. (A54) yields the coefficients for a generalized gyro data frequency-response function. It is also recognized that although Eq. (A54) is a general formulation, for specific frequency-response functions, the series expansions are usually computed and equated term by term without explicit recourse to derivative functions.

Conclusions

The preceding discussion shows techniques for tuning coning algorithms to gyro data with frequency responses deviating from the normally assumed flat response. The high-order achieved by previously published coning algorithms is usually lost if such algorithms are applied to nonideal or filtered gyro data. The coning algorithm tuning procedure shown here permits the development of algorithms that achieve high-order response using filtered gyro data. In addition, the technique can be used in general to tune coning algorithms to gyro characteristics deviating from the ideal condition, as is often the case in mechanical gyroscopes. Coning algorithms for filtered or shaped data can be implemented in exactly the same form as for unfiltered data. The only change required is the tuning of the VCP coefficients to match the gyro data frequency response. Numerous advantages can be gained using the techniques described. These include the possibility of using high-order algorithms with gyros having nonideal response or the deliberate use of filtering to eliminate undesired high-frequency content that can lead to pseudoconing. The use of filtered data with the coning algorithms described permits a very sharp cutoff at the Nyquist frequency with substantially reduced overshoot and overcompensation at frequencies above Nyquist along with very high-order response in the frequency ranges of interest.

Appendix: Derivation of Coning Algorithms

Coning Motion

A pure coning motion can be represented in terms of the vector angle $\boldsymbol{\phi}$, where

$$\boldsymbol{\phi} = \varepsilon \sin(\omega t)\boldsymbol{i} + \varepsilon \cos(\omega t)\boldsymbol{j} \tag{A1}$$

where ε is the cone half-angle, ω is the angular frequency, and t is time. The unit vectors $\boldsymbol{i}$ and $\boldsymbol{j}$ are orthogonal and normal to the Euler axis. The coning motion can also be represented by the quaternion $\tilde{q}$, where

$$\tilde{q} = \{\cos(\varepsilon/2), \sin(\varepsilon/2)[\sin(\omega t)\boldsymbol{i} + \cos(\omega t)\boldsymbol{j}]\} \tag{A2}$$

The angular rate vector $\boldsymbol{\Omega}$ can be found using the quaternion differential equation

$$\frac{\mathrm{d}\tilde{q}}{\mathrm{d}t} = \frac{1}{2}\tilde{q}\boldsymbol{\Omega} \tag{A3}$$

or

$$\boldsymbol{\Omega} = 2\tilde{q}^* \frac{\mathrm{d}q}{\mathrm{d}t} \tag{A4}$$

where the asterisk denotes the conjugate of the quaternion wherein the vector components are reversed in sign:

$$\boldsymbol{\Omega} = 2\{\cos(\varepsilon/2), -\sin(\varepsilon/2)[\sin(\omega t)\boldsymbol{i} + \cos(\omega t)\boldsymbol{j}]\}\omega \times \{0, \sin(\varepsilon/2)[\cos(\omega t)\boldsymbol{i} - \sin(\omega t)\boldsymbol{j}]\} \tag{A5}$$

$$\boldsymbol{\Omega} = \omega[0, \sin\varepsilon \cos(\omega t)\boldsymbol{i} - \sin\varepsilon \sin(\omega t)\boldsymbol{j} + 2\sin^2(\varepsilon/2)\boldsymbol{k}] \tag{A6}$$

The gyro incremental angle output is given by

$$\Delta\boldsymbol{\theta} = \int_{\left(n-\frac{1}{2}\right)\Delta t}^{\left(n+\frac{1}{2}\right)\Delta t} \boldsymbol{\Omega}\,\mathrm{d}t \tag{A7}$$

$$\Delta\boldsymbol{\theta} = \omega\Delta t\{\sin\varepsilon\,\mathrm{sinc}(\omega\Delta t/2)[\cos(n\omega\Delta t)\boldsymbol{i} - \sin(n\omega\Delta t)\boldsymbol{j}] + 2\sin^2(\varepsilon/2)\boldsymbol{k}\} \tag{A8}$$

where, as commonly defined, $\mathrm{sinc}(x) \equiv \sin(x)/x$.

In strapdown systems, the quaternion is updated using a transition quaternion derived from the gyro incremental angle outputs. However, the exact transition quaternion can be computed for the coning motion using the expressions

$$\tilde{q}^{n+\frac{1}{2}} = \tilde{q}^{n-\frac{1}{2}}\tilde{q}(\Delta\boldsymbol{\phi}) \qquad \text{or} \qquad \tilde{q}(\Delta\boldsymbol{\phi}) = \tilde{q}^{*n-\frac{1}{2}}\tilde{q}^{n+\frac{1}{2}} \tag{A9}$$

$$\tilde{q}(\Delta\boldsymbol{\phi}) = \left(\cos(\varepsilon/2), -\sin(\varepsilon/2)\left\{\sin\left[\left(n-\tfrac{1}{2}\right)\omega\Delta t\right]\boldsymbol{i} + \cos\left[\left(n-\tfrac{1}{2}\right)\omega\Delta t\right]\boldsymbol{j}\right\}\right)\left(\cos(\varepsilon/2), \sin(\varepsilon/2)\left\{\sin\left[\left(n+\tfrac{1}{2}\right)\omega\Delta t\right]\boldsymbol{i} + \cos\left[\left(n+\tfrac{1}{2}\right)\omega\Delta t\right]\boldsymbol{j}\right\}\right) \tag{A10}$$

$$\tilde{q}(\Delta\boldsymbol{\phi}) = \{\cos^2(\varepsilon/2) + \sin^2(\varepsilon/2)\cos(\omega\Delta t), \sin\varepsilon\sin(\omega\Delta t/2) \times [\cos(n\omega\Delta t)\boldsymbol{i} - \sin(n\omega\Delta t)\boldsymbol{j}] + \sin^2(\varepsilon/2)\sin(\omega\Delta t)\boldsymbol{k}\} \tag{A11}$$

Now

$$\tilde{q}(\Delta\boldsymbol{\phi}) = [\cos(|\Delta\boldsymbol{\phi}|/2), \sin(|\Delta\boldsymbol{\phi}|/2)\,\mathbf{1}_{\Delta\phi}] \tag{A12}$$

Hence,

$$\Delta\boldsymbol{\phi} = 2\frac{\sin^{-1}(|\Delta\boldsymbol{\phi}|/2)}{\sin(|\Delta\boldsymbol{\phi}|/2)}\left(\sin\frac{|\Delta\boldsymbol{\phi}|}{2}\mathbf{1}_{\Delta\phi}\right) \tag{A13}$$

Equating the magnitudes of the vector parts of Eqs. (A11) and (A12) yields

$$\sin(|\Delta\boldsymbol{\phi}|/2) = \sqrt{\sin^2\varepsilon\sin^2(\omega\Delta t/2) + \sin^4(\varepsilon/2)\sin^2(\omega\Delta t)} \tag{A14}$$

Utilizing a series expansion $\sin^{-1}x/x \cong 1 + \frac{1}{3!}x^2 + \cdots$ yields the following approximation for Eq. (A13):

$$\Delta\boldsymbol{\phi} = \mathrm{SF}\,\omega\Delta t[\sin\varepsilon\,\mathrm{sinc}(\omega\Delta t/2)\cos(n\omega\Delta t)\boldsymbol{i} - \sin\varepsilon\,\mathrm{sinc}(\omega\Delta t/2)\sin(n\omega\Delta t)\boldsymbol{j} + 2\sin^2(\varepsilon/2)\,\mathrm{sinc}\,\omega\Delta t\boldsymbol{k}] \tag{A15}$$

where

$$\mathrm{SF} = \frac{\sin^{-1}(|\Delta\phi|/2)}{\sin(|\Delta\phi|/2)} \approx 1 + \frac{1}{3!}\left[\sin^2\varepsilon\sin^2\frac{\omega\Delta t}{2} + \sin^4\frac{\varepsilon}{2}\sin^2(\omega\Delta t)\right] \tag{A16}$$

Note that the scale factor (SF) is basically dependent only on the magnitude of $(\Delta\boldsymbol{\phi})^2$ or $(\Delta\boldsymbol{\theta})^2$ and is bounded by $[(|\boldsymbol{\Omega}|/2)\Delta t]^2$ and not really by ε or ω, as will be shown. From Eq. (A6),

$$(|\boldsymbol{\Omega}|/2)\Delta t = \omega\Delta t\sin(\varepsilon/2) \tag{A17}$$

and

$$\begin{aligned}\sin^2\varepsilon\sin^2(\omega\Delta t/2) + \sin^4(\varepsilon/2)\sin^2(\omega\Delta t) &= (\omega\Delta t)^2\sin^2(\varepsilon/2)\,\mathrm{sinc}^2(\omega\Delta t/2)[1 - \sin^2(\varepsilon/2)\sin^2(\omega\Delta t/2)]\\ &= [(|\boldsymbol{\Omega}|/2)\Delta t]^2\,\mathrm{sinc}^2(\omega\Delta t/2)[1 - \sin^2(\varepsilon/2)\sin^2(\omega\Delta t/2)]\\ &\le [(|\boldsymbol{\Omega}|/2)\Delta t]^2\end{aligned} \tag{A18}$$

We will ignore the effect of the SF in the remainder of this discussion because, in practice, the bound is small. Thus, the target $\Delta\boldsymbol{\phi}$ desired for updating the quaternion is given by

$$\Delta\boldsymbol{\phi} = \omega\Delta t[\sin\varepsilon\,\mathrm{sinc}(\omega\Delta t/2)\cos(n\omega\Delta t)\boldsymbol{i} - \sin\varepsilon\,\mathrm{sinc}(\omega\Delta t/2)\sin(n\omega\Delta t)\boldsymbol{j} + 2\sin^2(\varepsilon/2)\,\mathrm{sinc}\,\omega\Delta t\,\boldsymbol{k}] \tag{A19}$$

Coning Compensation

The normal method of deriving coning algorithms introduced by Miller[3] is to concentrate on the fact that the main difference between $\Delta\boldsymbol{\phi}$ and $\Delta\boldsymbol{\theta}$ is in the z component. Thus, we want

$$\Delta\theta_z + \text{compensation} \cong \Delta\phi_z \qquad \text{or}$$

$$\text{compensation} \cong 2\sin^2(\varepsilon/2)(\operatorname{sinc}\omega\Delta t - 1)\omega\Delta t \quad \text{(A20)}$$

The compensation is obtained by employing cross products of $\Delta\boldsymbol{\theta}$ from subintervals.

Filtered Data

Now suppose that

$$\Delta\boldsymbol{\theta} = \omega\Delta t\{F(\omega)\sin\varepsilon\operatorname{sinc}(\omega\Delta t/2)[\cos(n\omega\Delta t)\boldsymbol{i} - \sin(n\omega\Delta t)\boldsymbol{j}] + 2F(0)\sin^2(\varepsilon/2)\boldsymbol{k}\} \quad \text{(A21)}$$

where $F(\omega)$ is a digital filter function for which

$$F(0) = 1, \qquad \lim_{\omega\to 0} F(\omega) = 1, \qquad |F(\omega)| \le F_{\max} \quad \text{for all } \omega \quad \text{(A22)}$$

Equivalent Cone

We now consider a coning motion where the cone angle is a function of frequency, that is, $\varepsilon = \varepsilon_0 g(\omega)$. Then the desired vector angle $\Delta\,\boldsymbol{\phi}$ is approximately given by Eq. (A15):

$$\Delta\,\boldsymbol{\phi} = \omega\Delta t\{\sin[\varepsilon_0 g(\omega)]\operatorname{sinc}(\omega\Delta t/2)[\cos(n\omega\Delta t)\boldsymbol{i} - \sin(n\omega\Delta t)\boldsymbol{j}] + 2\sin^2[\varepsilon_0 g(\omega)/2]\operatorname{sinc}\omega\Delta t\,\boldsymbol{k}\} \quad \text{(A23)}$$

We now equate the time-varying (ac) parts of Eqs. (A21) and (A23) and obtain the following:

$$F(\omega)\sin\varepsilon = \sin[g(\omega)\varepsilon_0] \quad \text{(A24a)}$$

and solving for $g(\omega)$,

$$g(\omega) = (1/\varepsilon_0)\sin^{-1}[F(\omega)\sin\varepsilon] \quad \text{(A24b)}$$

The function $g(\omega)$ defines the apparent cone resulting from the filtered data. The term appearing in the third time-invariant (dc) component of Eq. (A23) is scaled by the factor

$$\sin^2[\varepsilon_0 g(\omega)/2] = \{1 - \cos[\varepsilon_0 g(\omega)]\}/2 = (1 - \cos\{\sin^{-1}[F(\omega)\sin\varepsilon]\})/2 \quad \text{(A25)}$$

For either small ω or small ε, the preceding factor can be approximated by

$$\sin^2[\varepsilon_0 g(\omega)/2] \approx F^2(\omega)\sin^2(\varepsilon/2) \quad \text{(A26)}$$

Substituting Eqs. (A24) and (A26) into Eq. (A23) yields the desired $\Delta\,\boldsymbol{\phi}$:

$$\Delta\,\boldsymbol{\phi} = \omega\Delta t\{F(\omega)\sin\varepsilon\operatorname{sinc}(\omega\Delta t/2)[\cos(n\omega\Delta t)\boldsymbol{i} - \sin(n\omega\Delta t)\boldsymbol{j}] + 2F^2(\omega)\sin^2(\varepsilon/2)\operatorname{sinc}(\omega\Delta t)\boldsymbol{k}\} \quad \text{(A27)}$$

The compensation is the difference between the $\boldsymbol{k}$ components of Eqs. (A27) and (A21).

$$\text{compensation} \cong 2\omega\Delta t\sin^2(\varepsilon/2)[F^2(\omega)\operatorname{sinc}\omega\Delta t - F(0)] \cong 2\omega\Delta t\sin^2(\varepsilon/2)[F^2(\omega)\operatorname{sinc}\omega\Delta t - 1] \quad \text{(A28)}$$

Note that Eq. (A28) collapses into Eq. (A20) when $F(\omega) = 1$.

Generalized Miller Method[3]

The generalized Miller method[3] breaks up each quaternion update interval into m subintervals of duration Δt. A $\Delta\,\boldsymbol{\theta}$ is obtained in each subinterval and VCPs formed between the subinterval $\Delta\,\boldsymbol{\theta}$'s according to their spacing in time. For example, with $m = 4$, subinterval spacings of 1, 2, and 3 are possible. A one-subinterval spacing results in the category-1 cross products $\Delta\,\boldsymbol{\theta}_1 \times \Delta\,\boldsymbol{\theta}_2$, $\Delta\,\boldsymbol{\theta}_2 \times \Delta\,\boldsymbol{\theta}_3$, and $\Delta\,\boldsymbol{\theta}_3 \times \Delta\,\boldsymbol{\theta}_4$. A two-subinterval spacing results in the category-2 cross products $\Delta\,\boldsymbol{\theta}_1 \times \Delta\,\boldsymbol{\theta}_3$ and $\Delta\,\boldsymbol{\theta}_2 \times \Delta\,\boldsymbol{\theta}_4$. A three-subinterval spacing results in the category-3 cross product $\Delta\,\boldsymbol{\theta}_1 \times \Delta\,\boldsymbol{\theta}_4$.

In general, there will be $m - 1$ possible subinterval spacings and C_m^2 possible cross products. Each category of cross products is described by the quantity $C_p(n)$, where

$$C_p(n) = (\Delta\boldsymbol{\theta}_{nm} \times \Delta\boldsymbol{\theta}_{nm+p})_{k\text{th component}} \quad \text{(A29)}$$

It can be shown that all cross products with the same spacing have the same $\boldsymbol{k}$ component. The ac components, that is, $\boldsymbol{i}$ and $\boldsymbol{j}$, have only higher-order terms, that is, ε^3 and $F^3(\omega)$, and can be ignored.

Returning to Eq. (A21) and appropriately substituting into the preceding expression yields

$$C_p(n) = -(\omega\Delta t)^2 F^2(\omega)\sin^2\varepsilon\operatorname{sinc}^2(\omega\Delta t/2)\sin(p\omega\Delta t) \quad \text{(A30)}$$

Note that this expression does not depend on n.

Coning Algorithm for Resolution-Enhanced Data (Example)

In the case of resolution-enhanced data,[8]

$$F(\omega) \cong \operatorname{sinc}(\omega\Delta t/2) \quad \text{(A31)}$$

It follows that

$$C_p(n) \cong -(\omega\Delta t)^2\sin^2\varepsilon\operatorname{sinc}^4(\omega\Delta t/2)\sin(p\omega\Delta t) \quad \text{(A32)}$$

Let $\alpha = \omega\Delta t$; then

$$C_p(n) \cong -\alpha^2\sin^2\varepsilon\operatorname{sinc}^4(\alpha/2)\sin(p\alpha) \quad \text{(A33)}$$

Now

$$\operatorname{sinc}^4\frac{\alpha}{2} = \alpha^{-4}[6 - 8\cos\alpha + 2\cos(2\alpha)] \quad \text{(A34)}$$

$$\begin{aligned} C_p(n) &\cong -\frac{\sin^2\varepsilon}{\alpha^2}[6 - 8\cos\alpha + 2\cos(2\alpha)]\sin(p\alpha) \\ &\cong -\frac{\sin^2\varepsilon}{\alpha^2}\{\sin[(p-2)\alpha] - 4\sin[(p-1)\alpha] + 6\sin(p\alpha) - 4\sin[(p+1)\alpha] + \sin[(p+2)\alpha]\} \\ &\cong -\frac{\sin^2\varepsilon}{\alpha^2}\left\{\sum_{k=1}^{\infty}(-1)^k[(p-2)^{2k-1} - 4(p-1)^{2k-1} + 6p^{2k-1} - 4(p+1)^{2k-1} + (p+2)^{2k-1}]\frac{\alpha^{2k-1}}{(2k-1)!}\right\} \end{aligned} \quad \text{(A35)}$$

Evaluating the $k = 1$ and $k = 2$ terms of the sum reveals that these are zero for any value of p. Thus, the sum reduces to

$$C_p(n) \cong \frac{\sin^2\varepsilon}{\alpha^2}\left\{\sum_{k=1}^{\infty}(-1)^k[(p-2)^{2k+3} - 4(p-1)^{2k+3} + 6p^{2k+3} - 4(p+1)^{2k+3} + (p+2)^{2k+3}]\frac{\alpha^{2k+3}}{(2k+3)!}\right\} \quad \text{(A36)}$$

Returning to Eq. (A28), which gives the desired compensation, we obtain

$$\text{desired compensation} \cong 2\omega m\Delta t\sin^2(\varepsilon/2)[F^2(\omega)\operatorname{sinc}\omega m\Delta t - 1] \quad \text{(A37)}$$

For resolution-enhanced data, we substitute Eq. (A31) to yield

$$\text{desired compensation} \cong -2\omega m\Delta t\sin^2(\varepsilon/2) \times [1 - \operatorname{sinc}^2(\omega\Delta t/2)\operatorname{sinc}\omega m\Delta t] \quad \text{(A38)}$$

The bracketed expression in the preceding equation is expanded by means of trigonometric identities:

$$[\,] = 1 - \frac{4}{m\alpha^3}\left(\frac{1-\cos\alpha}{2}\right)\sin(m\alpha) = 1 - \frac{1}{m\alpha^3}\{-\sin[(m-1)\alpha] + 2\sin(m\alpha) - \sin[(m+1)\alpha]\}$$
$$= 1 - \frac{1}{m\alpha^3}\sum_{k=1}^{\infty}(-1)^k[(m-1)^{2k-1} - 2m^{2k-1} + (m+1)^{2k-1}]\frac{\alpha^{2k-1}}{(2k-1)!} \tag{A39}$$

For $k=1$, the expression within the sum vanishes. For $k=2$, the expression corresponding to the sum is 1. Thus, the bracketed expression can be rewritten as

$$[\,] = \frac{1}{m}\sum_{k=1}^{\infty}(-1)^{k+1}[(m-1)^{2k+3} - 2m^{2k+3} + (m+1)^{2k+3}]\frac{\alpha^{2k}}{(2k+3)!} \tag{A40}$$

Finally, substituting Eq. (A40) into Eq. (A38) yields

$$\text{desired compensation} = 2\omega\Delta t\sin^2\frac{\varepsilon}{2}\sum_{k=1}^{\infty}(-1)^k[(m-1)^{2k+3} - 2m^{2k+3} + (m+1)^{2k+3}]\frac{\alpha^{2k}}{(2k+3)!} \tag{A41}$$

Note that for $m=1$ no compensation is possible and that the net error will be the negative of the desired compensation. The lowest-order term, expressed as a rate, will be

$$\text{error rate} = -\tfrac{1}{2}\omega\sin^2(\varepsilon/2)(\omega\Delta t)^2 \tag{A42}$$

For $m > 1$, cross products may be found and applied as compensation. Linear combinations of the $(m-1)$ categories of cross products are found that equal up to the $(m-1)$th term of the desired compensation equation. Thus, coefficients x_p are chosen such that

$$\sum_{p=1}^{m-1}C_p x_p = 2\omega\Delta t\sin^2\frac{\varepsilon}{2}\sum_{k=1}^{\infty}(-1)^k[(m-1)^{2k+3} - 2m^{2k+3} + (m+1)^{2k+3}]\frac{\alpha^{2k}}{(2k+3)!} \tag{A43}$$

This is equivalent to the following system of equations [using Eqs. (A36) and (A43)]:

$$\sin^2\varepsilon\sum_{p=1}^{m-1}\left\{[(p-2)^{2k+3} - 4(p-1)^{2k+3} + 6p^{2k+3} - 4(p+1)^{2k+3} + (p+2)^{2k+3}]x_p\right\} = 2\sin^2\frac{\varepsilon}{2}[(m-1)^{2k+3} - 2m^{2k+3} + (m+1)^{2k+3}]$$
$$\text{with } k = 1, \ldots, m-1 \tag{A44}$$

Under the assumption of a small ε, Eqs. (A44) further reduce to

$$2\sum_{p=1}^{m-1}\left\{[(p-2)^{2k+3} - 4(p-1)^{2k+3} + 6p^{2k+3} - 4(p+1)^{2k+3} + (p+2)^{2k+3}]x_p\right\} = [(m-1)^{2k+3} - 2m^{2k+3} + (m+1)^{2k+3}] \tag{A45}$$

For $k = 1, \ldots, m-1$, this leads to $m-1$ equations with $m-1$ unknowns $(x_1, \ldots, x_{m-1})$.

Once the compensation has been applied, a residual error exists, which is the remaining portion of the desired compensation. The largest-order term is the mth term of the difference between the compensation series and the desired series. This can be converted to a rate by dividing by $m\Delta t$. The relative error rate (i.e., error rate normalized to coning rate) will be of order $2m$ in $\omega\Delta t$.

The calculated coning coefficients x_p are given in Table 2 for several values of m. Computer simulations of present-day coning algorithms yielded the response graphs shown in Figs. 2 and 4. Computer simulations of the coning algorithms described yielded the response graphs shown in Figs. 3 and 5. The results for large angular rates are shown in Fig. 6.

Formulation for General Filter Function

When Eq. (A38) is returned to, the desired compensation for small angles can be expressed as

$$\text{desired compensation} \cong \tfrac{1}{2}m\alpha\varepsilon^2[F^2(\alpha)\,\text{sinc}\,m\alpha - 1] \tag{A46}$$

where α has been substituted for $\omega\Delta t$. The applied compensation according to Eq. (A30) is

$$\text{applied compensation} \cong \sum_{p=1}^{m-1}C_p x_p = -\alpha^2\varepsilon^2F^2(\alpha)\,\text{sinc}^2\frac{\alpha}{2}\sum_{p=1}^{m-1}\sin(p\alpha)x_p \tag{A47}$$

In comparing Eqs. (A46) and (A47), it is apparent that $\alpha\varepsilon^2$ appears in both. Hence, we define the following:

$$z(\alpha) = \tfrac{1}{2}m[F^2(\alpha)\,\text{sinc}\,m\alpha - 1] \tag{A48}$$

The quantity $z(\alpha)$ is clearly an even function of α and may be expanded into a Taylor series about $\alpha = 0$:

$$z(\alpha) = \frac{1}{2}m\sum_{k=0}^{\infty}\frac{\alpha^{2k}}{(2k)!}\frac{d^{2k}}{d\alpha^{2k}}[F^2(\alpha)\,\text{sinc}\,m\alpha - 1]|_{\alpha=0} \tag{A49}$$

Since

$$\lim_{\alpha\to 0}F(\alpha) = 1$$

the $k=0$ term of the equation is zero. Consequently,

$$z(\alpha) = \frac{1}{2}m\sum_{k=1}^{\infty}\frac{\alpha^{2k}}{(2k)!}\frac{d^{2k}}{d\alpha^{2k}}[F^2(\alpha)\,\text{sinc}\,m\alpha]|_{\alpha=0} \tag{A50}$$

We also define

$$y(\alpha) = \frac{1}{\alpha\varepsilon^2}\sum_{p=1}^{m-1}C_p x_p = -\alpha F^2(\alpha)\,\text{sinc}^2\frac{\alpha}{2}\sum_{p=1}^{m-1}\sin(p\alpha)x_p \tag{A51}$$

This is also an even function of α and may be expanded into a Taylor series,

$$y(\alpha) = -\sum_{p=1}^{m-1}\left\{\sum_{k=0}^{\infty}\frac{\alpha^{2k}}{(2k)!}\frac{d^{2k}}{d\alpha^{2k}}\left[\alpha F^2(\alpha)\,\text{sinc}^2\frac{\alpha}{2}\sin(p\alpha)\right]\Bigg|_{\alpha=0}\right\}x_p \tag{A52}$$

The $k=0$ term of the internal summation is zero and, consequently,

$$y(\alpha) = -\sum_{p=1}^{m-1}\left\{\sum_{k=1}^{\infty}\frac{\alpha^{2k}}{(2k)!}\frac{d^{2k}}{d\alpha^{2k}}\left[\alpha F^2(\alpha)\,\text{sinc}^2\frac{\alpha}{2}\sin(p\alpha)\right]\Bigg|_{\alpha=0}\right\}x_p \tag{A53}$$

We now equate the first $(m-1)$ terms of the k series of Eqs. (A50) and (A53) to yield $m-1$ equations with $m-1$ unknowns, $x_1, x_2, \ldots, x_{m-1}$. For $k=1$ to $k=m-1$,

$$\sum_{p=1}^{m-1}\frac{d^{2k}}{d\alpha^{2k}}\left[\alpha F^2(\alpha)\,\text{sinc}^2\frac{\alpha}{2}\sin(p\alpha)\right]\Bigg|_{\alpha=0}x_p = -\frac{1}{2}m\frac{d^{2k}}{d\alpha^{2k}}[F^2(\alpha)\,\text{sinc}\,m\alpha]|_{\alpha=0} \tag{A54}$$

The solution to these equations leads to the cancellation of all terms of order $2m - 2$ and below, leaving terms of order $2m$ in the relative error rate. This type of analysis may be used for a variety of filter functions $F(\omega)$ including low-pass filters of many forms.

Acknowledgment

This paper is based on “Application of Coning Algorithms to Frequency Shaped Data,” presented by the authors at the 6th Saint Petersburg International Conference on Integrated Navigation Systems, Saint Petersburg, Russia, 24–26 May 1999.

References

[1]Goodman, L. E., and Robinson, A. R., “Effect of Finite Rotations on Gyroscopic Sensing Devices,” American Society of Mechanical Engineers, ASME Paper 57-A-30, 1957.

[2]Bortz, J. E., “A New Mathematical Formulation for Strapdown Inertial Navigation,” *IEEE Transactions on Aerospace and Electronic Systems*, Vol. 7, No. 1, 1971, pp. 61–66.

[3]Miller, R. B., “A New Strapdown Attitude Algorithm,” *Journal of Guidance, Control, and Dynamics*, Vol. 6, No. 4, 1983, pp. 287–291.

[4]Ignagni, M. B., “Optimal Strapdown Attitude Integration Algorithms,” *Journal of Guidance, Control, and Dynamics*, Vol. 13, No. 2, 1990, pp. 363–369.

[5]Lee, J. G., Yoon, Y. J., Mark, J. G., and Tazartes, D. A., “Extension of Strapdown Attitude Algorithm for High-Frequency Base Motion,” *Journal of Guidance, Control, and Dynamics*, Vol. 13, No. 4, 1990, pp. 738–743.

[6]Litmanovich, Y. A., “Use of Angular Rate Multiple Integrals as Input Signals for Strapdown Attitude Algorithms,” *Proceedings of Symposium Gyro Technology*, Univ. of Stuttgart, Stuttgart, Germany, 1997.

[7]Savage, P. G., “Strapdown Inertial Navigation Integration Algorithm Design Part 1: Attitude Algorithms,” *Journal of Guidance, Control, and Dynamics*, Vol. 21, No. 1, 1998, pp. 19–27.

[8]Mark, J. G., and Tazartes, D. A., “Resolution Enhancement Technique for Laser Gyroscopes,” *Proceedings of 4th International Conference on Integrated Navigation Systems*, St. Petersburg, 1997, pp. 378–387.